PERGAMON

International Journal of Solids and Structures 40 (2003) 1633–1651

INTERNATIONAL JOURNAL OF SOLIDS and STRUCTURES

www.elsevier.com/locate/ijsolstr

Effect of debonding in active constrained layer damping patches on hybrid control of smart beams

Dongchang Sun, Liyong Tong *

School of Aerospace, Mechanical and Mechatronic Engineering, The University of Sydney, NSW 2006, Australia

Received 24 June 2002; received in revised form 18 November 2002

Abstract

A new model for a smart beam with a partially debonded active constrained layer damping (ACLD) patch is presented, and the effects of the debonding of the ACLD patch on both passive and hybrid control are investigated. In this model, both shear and compressional vibrations of the viscoelastic material (VEM) layer are considered. The moment inertia and the transverse shear effect are also taken into account based on the Timoshenko's beam theory. The adhesive layer between the host beam and the piezoelectric sensor patch is modeled as an elastic load transferring media. The debonding of the ACLD patch is approximated by removing the VEM between the constraining layer and the host beam in the debonding region, and the continuity conditions are imposed based on displacement continuity and force balance. A modal velocity observer-based modal control scheme is also given to perform the active modal control of the beam. In order to examine the effects of part debonding of the ACLD patch, the characteristic equation of the beam treated with an ACLD patch is derived. The simulation example results show that an edge debonding of the ACLD patch can significantly affect both passive and hybrid control. It is also found that the additional mode induced by the debonding has unique effects on the modal damping ratios and frequencies of both open-loop and closed-loop system.

Keywords: Debonding; Active constrained layer damping; Hybrid control; Piezoelectric transducers

1. Introduction

With the development of technology, vibration and noise control become increasingly important in various machinery and structure design, and more accurate active control is needed in defense and aerospace industries. Therefore, it becomes a significant challenge to precisely control the vibration of flexible structures.

Passive damping treatment is a traditional method to suppress vibration of structures (Douglas and Yang, 1969). Constrained layer damping treatment is an effective way to provide significant passive damping, which includes a viscoelastic material (VEM) layer sandwiched between a constraining layer and

* Corresponding author. Tel.: +61-2-9351-6949; fax: +61-2-9351-4841.
E-mail address: ltong@aeromech.usyd.edu.au (L. Tong).

0020-7683/02/$ - see front matter © 2002 Elsevier Science Ltd. All rights reserved.
doi:10.1016/S0020-7683(02)00672-8

the structure to be damped. The passive constrained layer damping (PCLD) treatment has been widely used in various fields due to its unconditional stability. In spite of their safety feature, passive damping can only produce unadjustable damping in a limited range.

The recently developed smart/intelligent structure technology (Crawley, 1994; Rao and Sunar, 1994; Chee et al., 1998) has great potential in precise vibration control of flexible structures such as thin plates and shells. Piezoelectric materials such as ceramic lead zirconate titanate (PZT) and polymer polyvinylidence fluoride (PVDF) are the most commonly used materials for distributed actuators and sensor due to their characteristics of quick response, low power consumption and high linearity. Since distributed sensors and actuators are used to replace traditional point sensors and actuators, more dimensions has been added to active control, and hence more precise control can be achieved.

Combined the smart structures technology and passive control, an innovative concept, the active constrained layer damping (ACLD) treatment (Baz, 1993; Shen, 1994; Shen, 1996; Kapadia and Kawiecki, 1997; Liao and Wang, 1997; Chattopadhyay et al., 2001; Shi et al., 2001; Lee and Kim, 2001) in vibration control of flexible structures, has been proposed. A typical ACLD consists of a VEM layer sandwiched between the host structure and the active constraining layer, which is made of smart materials such as piezoelectric ceramics and magnets rather than conventional materials. The active layer can function as a conventional constraining layer to enhance the energy dissipation by enlarging the shear strain in the damping layer. On the other hand, the active layer is also used as the actuator to perform active control. Both passive and active control can be performed in the ACLD treatment, which consequently allows achievement of better control results and greatly improves robustness and reliability of the closed control system. Since the ACLD treatment has both active and passive control components, it makes the active control system more robust, more reliable to uncertainties, and it can also increase gain and phase margins, enhance the practicality, decrease power consumption and improve high frequency responses.

However, the fail-safe feature of the ACLD treated structures faces increasingly with new challenges, such as possible debonding of the ACLD layer. Due to emerging application of new high performance piezoelectric materials capable of generating large strain subject to a high electric field, the possibility of debonding of a piezoelectric actuator and a VEM layer from a host structure greatly increases, particularly, for the dynamic circumstances. In addition, fatigue and sudden electrical and mechanical loads may also cause debonding of the piezoelectric layers/patches. When a debonding between an ACLD layer and a host structure occurs, as depicted in Fig. 1, it will result in significant changes of the structural behavior particularly for closed-loop control, and may even destabilize the closed-loop control (Seeley and Chattopadhyay, 1998; Tylikowski, 2001; Sun et al., 2001). Thus, investigation into the effects of the ACLD debonding on active and passive control of smart structures is of great significance.

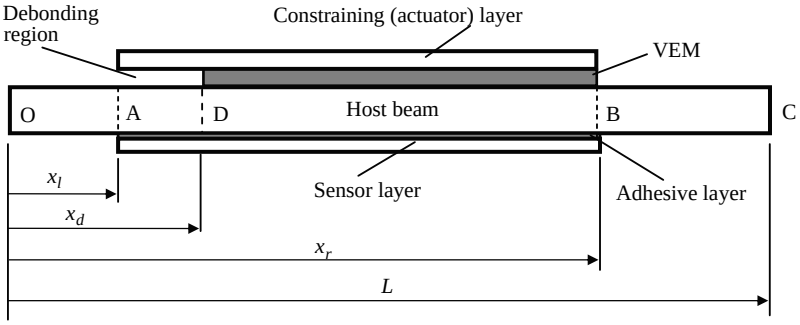

Fig. 1. Beam with partially debonded ACLD patches.

In all available models of ACLD treated structures, one of the fundamental assumptions is that the active constraining layer and the host structure have the same transverse displacement, namely, the VEM layer does not undergo peel strain. Apparently, when a debonding in the ACLD layer occurs, this assumption is no longer valid because the active constraining layer and the host structure vibrate separately in the debonding region. Therefore, the existing theories are not capable of modeling the debonding of the ACLD layers.

In this paper, a new model of an ACLD treated beam is presented to investigate the effects of the partially debonded ACLD patch on both passive and hybrid control. In this model, both shear and compressional vibration of the VEM layer are taken into account. The debonding of the ACLD patch is modeled by removing the VEM between the constraining layer and the host beam in the debonding region, and corresponding displacement continuity conditions and force balance conditions are also imposed. In order to examine the effects of part debonding of the ACLD patch on passive and active control, a characteristic equation of a beam with an ACLD patch is derived. Based on the model and the characteristic equation, the effects of the debonding in the ACLD patch on both passive and active control are studied through a simulation example.

2. Mathematical model

2.1. Basic equations based on Timoshenko's beam theory

Consider a beam of length L and width b treated with an ACLD patch with different thickness and length, as shown in Fig. 1. The ACLD patch consists of a piezoelectric constraining layer (actuator) together with a VEM layer bonded on the upper surface of the host beam, and a piezoelectric sensor layer on the lower surface. In the following derivation, assume the effects of the adhesive layers on the VEM layer can be neglected. The VEM layer and the adhesive layer between the sensor and the host beam are assumed to carry constant transverse shear and peel strains across its thickness at a given point. Assume that all debondings in the ACLD patches occur throughout the entire width of the beam. In the debonded region, it is assumed that there is no stress transferring between the host beam and piezoelectric constraining layer, and that the damping effect of the debonded VEM layer can be negligible due to its small shear and normal strains. In other words, the debonding of the ACLD is modeled by neglecting the thin VEM layer because it is light and soft.

Since the beam is partly covered by the ACLD patch, the governing equations should be derived in segment. For the segment AB of the beam covered with the ACLD patch, by applying the Timoshenko's beam theory, the equations of motion can be derived as follows:

$$\begin{aligned}
&\rho_1 b h_1 u_{1,tt} = T_{1,x} + b\tau_{\mathrm{v}}, \quad \rho_1 b h_1 w_{1,tt} = Q_{1,x} + b\sigma_{\mathrm{v}}, \quad \rho_1 J_1 \psi_{1,tt} = M_{1,x} + b\tau_{\mathrm{v}} h_1/2 - Q_1,\\
&\rho_2 b h_2 u_{2,tt} = T_{2,x} - b\tau_{\mathrm{v}} + b\tau_{\mathrm{a}}, \quad \rho_2 b h_2 w_{2,tt} = Q_{2,x} - b\sigma_{\mathrm{v}} + b\sigma_{\mathrm{a}},\\
&\rho_2 J_2 \psi_{2,tt} = M_{2,x} + b(\tau_{\mathrm{v}} + \tau_{\mathrm{a}}) h_2/2 - Q_2, \quad \rho_3 b h_3 u_{3,tt} = T_{3,x} - b\tau_{\mathrm{a}},\\
&\rho_3 b h_3 w_{3,tt} = Q_{3,x} - b\sigma_{\mathrm{a}}, \quad \rho_3 J_3 \psi_{3,tt} = M_{3,x} + b\tau_a h_3/2 - Q_3
\end{aligned} \tag{1}$$

where the subscripts 1, 2, 3, v and a represent the piezoelectric constraining (actuator) layer, the host beam, the lower piezoelectric layer, the VEM layer and the adhesive layer between the sensor and the host beam, respectively, the subscript x stands for the partial derivative with respect to x, tt is the second derivative with respect to time t, u and w are the longitudinal and transverse displacements, h is the thickness, b is the width of the composite beam, τ and σ are shear and peel stresses, T, Q and M are the stress resultants, ρ is the equivalent mass densities, J is the moment of inertia, ψ is the rotation angle of the line element originally perpendicular to the longitudinal axis, which is given by

$$\psi_i = \gamma_i - w_{i,x}, \quad i = 1,2,3 \tag{2}$$

and γ_i is the shear strain at the neutral axis and has the form

$$\gamma_i = \frac{c_i Q_i}{G_i A_i}, \quad i = 1,2,3 \tag{3}$$

where c_i is a constant depending on the cross-sectional shape of the structural member. Note that the effects of both the transverse shear and the moment of inertia in the constraining layer, the host beam and the sensor layer are taken into account in Eq. (1).

The stress resultants and bending moments in Eq. (1) can be derived as follows;

$$\begin{aligned} T_1 &= E_1 b h_1 u_{1,x} - b e_{311} V(t), \quad M_1 = \frac{E_1 b h_1^3}{12}\psi_{1,x} \\ T_2 &= E_2 b h_2 u_{2,x}, \quad M_2 = \frac{E_2 b h_2^3}{12}\psi_{2,x} \\ T_3 &= E_3 b h_3 u_{3,x}, \quad M_3 = \frac{E_3 b h_3^3}{12}\psi_{3,x} \end{aligned} \tag{4}$$

where $V(t)$ is the uniformly distributed voltage applied on the actuator, E is the Young's modulus, e_{311} is the piezoelectric stress constant of the actuator layer.

The peel and shear stresses in the VEM layer can be expressed as

$$\begin{aligned} \tau_v(x,t) &= k_v G_v \circ \gamma_v = k_v \int_{-\infty}^{t} G_v(t-\tau)\frac{\partial \gamma_v(x,\tau)}{\partial \tau}\,\mathrm{d}\tau \\ \sigma_v(x,t) &= k_v E_v \circ \varepsilon_v = k_v \int_{-\infty}^{t} E_v(t-\tau)\frac{\partial \varepsilon_v(x,\tau)}{\partial \tau}\,\mathrm{d}\tau \end{aligned} \tag{5}$$

where $\circ$ denotes the convolution integral, $G_v(t)$ and $E_v(t)$ are the relaxation functions of the VEM layer subjected to shear and peel deformation, k_v is a parameter describing the bonding condition of the ACLD patch given by

$$k_v = \begin{cases} 0 & \text{debonding} \\ 1 & \text{perfect bonding} \end{cases} \tag{6}$$

In Eq. (5), $\gamma_v(x,t)$ and $\varepsilon_v(x,t)$ are the shear and peal strains given by

$$\begin{aligned} \gamma_v(x,t) &= \frac{1}{h_v}[u_2 - u_1 - (h_1\psi_1 + h_2\psi_2)/2 + h_v(w_{1,x} + w_{2,x})/2] \\ \varepsilon_v &= (w_2 - w_1)/h_v \end{aligned} \tag{7}$$

Note that $(w_{1,x} + w_{2,x})/2$ in the shear angle in Eq. (7) is used to replace $w_{,x}$ in the well established formula because of the difference between the transverse displacements in the constraining layer and the host beam. When all layers are assumed to have the same transverse displacement w, and the shear effect in the host beam and the constraining layer are not considered, the shear angle in Eq. (7) will be simplified to the well-known form, i.e. $\gamma_v = [u_2 - u_1 + (h_1 w_{,x} + h_2 w_{,x})/2 + h_v w_{,x}]/h_v$ (Shen, 1994).

The shear and peel stresses in the adhesive layer between the sensor and the host beam can be expressed as

$$\begin{aligned} \tau_a &= \frac{G_a}{h_a}[u_3 - u_2 - (h_2\psi_2 + h_3\psi_3)/2 + h_a(w_{2,x} + w_{3,x})/2] \\ \sigma_a &= \frac{E_a}{h_a}(w_3 - w_2) \end{aligned} \tag{8}$$

For the sensor patch bonded on the lower surface of the host beam, the charge output can be evaluated by

$$q(t) = \int_{x_l}^{x_r} be_{313} u_{3,x}\,\mathrm{d}x = be_{313}[u_3(x_r) - u_3(x_l)] \tag{9}$$

where e_{313} is the piezoelectric stress constant of the sensor, x_l and x_r are the coordinates of the left and right ends of the sensor along the x-direction shown in Fig. 1.

2.2. Nondimensionalized equations

By introducing the following nondimensional variables

$$\begin{aligned}
&\xi = \frac{x}{L}, \quad \tilde{u}_i = \frac{u_i}{h_2}, \quad \tilde{w}_i = \frac{w_i}{h_2}, \quad \widetilde{T}_i = \frac{T_i}{E_2 b h_2}, \quad \widetilde{Q}_i = \frac{Q_i}{E_2 b h_2}, \quad i = 1,2,3 \\
&\widetilde{M}_i = \frac{M_i}{E_2 b h_2^2/12}, \quad \tilde{t} = \frac{t}{L^2}\sqrt{\frac{E_2 h_2^2}{12\rho_2}}, \quad \widetilde{V}(t_n) = \frac{e_{311} V(t)}{E_2 h_2}
\end{aligned} \tag{10}$$

where the tilde represent the nondimensional variables, and denoting the following 12 independent parameters

$$\begin{aligned}
&\eta_i = \frac{\rho_i L^2}{E_2} \ (i = 1,2,3), \quad \alpha_2 = \frac{h_2}{L}, \quad \beta_i = \frac{E_i}{E_2}, \quad \varphi_i = \frac{h_i}{h_2}, \quad (i = 1,3) \\
&\varphi_v = \frac{h_v}{h_2}, \quad \varphi_a = \frac{h_a}{h_2}, \quad \beta_{ev} = \frac{E_v}{E_2}, \quad \beta_v = \frac{G_v}{E_2}, \quad \beta_a = \frac{E_a}{E_2}
\end{aligned} \tag{11}$$

Eqs. (1)–(8) can be transformed into the following nondimensional equations in terms of the nondimensional variables:

$$\begin{aligned}
&m_1 k_t^2 \ddot{\tilde{u}}_1 = \widetilde{T}_{1,\xi} + \tilde{\tau}_v; \quad m_1 k_t^2 \ddot{\tilde{w}}_1 = \widetilde{Q}_{1,\xi} + \tilde{\sigma}_v; \quad I_1 k_t^2 \ddot{\psi}_1 = \widetilde{M}_{1,\xi} + r_{t1}\tilde{\tau}_v - r_{q1}\widetilde{Q}_1 \\
&m_2 k_t^2 \ddot{\tilde{u}}_2 = \widetilde{T}_{2,\xi} - \tilde{\tau}_v + \tilde{\tau}_a; \quad m_2 k_t^2 \ddot{\tilde{w}}_2 = \widetilde{Q}_{2,\xi} - \tilde{\sigma}_v + \tilde{\sigma}_a; \quad I_2 k_t^2 \ddot{\psi}_2 = \widetilde{M}_{2,\xi} + r_{t2}(\tilde{\tau}_v + \tilde{\tau}_a) - r_{q2}\widetilde{Q}_2 \\
&m_3 k_t^2 \ddot{\tilde{u}}_3 = \widetilde{T}_{3,\xi} - \tilde{\tau}_a; \quad m_3 k_t^2 \ddot{\tilde{w}}_3 = \widetilde{Q}_{3,\xi} - \tilde{\sigma}_a; \quad I_3 k_t^2 \ddot{\psi}_3 = \widetilde{M}_{3,\xi} + r_{t3}\tilde{\tau}_a - r_{q3}\widetilde{Q}_3 \\
&\widetilde{T}_1 = \widetilde{A}_1 \tilde{u}_{1,\xi} - \widetilde{V}; \quad \widetilde{T}_2 = \widetilde{A}_2 \tilde{u}_{2,\xi}; \quad \widetilde{T}_3 = \widetilde{A}_3 \tilde{u}_{3,\xi} \\
&\widetilde{M}_i = \widetilde{D}_i \psi_{i,\xi}; \quad \tilde{w}_{i,\xi} = (\widetilde{G}_i \widetilde{Q}_i - \psi_i)/\alpha_2, \qquad (i = 1,2,3) \\
&\tilde{\tau}_v = k_v r_v \circ \left[\tilde{u}_2 - \tilde{u}_1 - p_{v1}\psi_1 - p_{v2}\psi_2 + p_{v3}\widetilde{Q}_1 + p_{v4}\widetilde{Q}_2\right]; \quad \tilde{\sigma}_v = k_v r_{ev} \circ (\tilde{w}_2 - \tilde{w}_1) \\
&\tilde{\tau}_a = r_a\left[\tilde{u}_3 - \tilde{u}_2 - p_{a1}\psi_2 - p_{a2}\psi_3 + p_{a3}\widetilde{Q}_2 + p_{a4}\widetilde{Q}_3\right]; \quad \tilde{\sigma}_a = r_{ea}(\tilde{w}_3 - \tilde{w}_2)
\end{aligned} \tag{12}$$

where the double dot represents the second order derivation with respect to the nondimensional time $\tilde{t}$, and the parameters can be expressed in terms of the independent parameters in Eq. (11) as follows:

$$
\begin{aligned}
&\alpha_i = \varphi_i\alpha_2, \quad m_i = \alpha_i\eta_i, \quad I_i = m_i\varphi_i^2\alpha_i, \quad r_{ti} = 6\varphi_i, \quad r_{qi} = \frac{12}{\alpha_2}\\
&\widetilde{A}_i = \alpha_i\beta_i, \quad \widetilde{D}_i = \alpha_i\beta_i\varphi_i^2, \quad \widetilde{G}_i = \frac{2c_i(1-v_i)}{\beta_i\varphi_i}, \qquad (i=1,2,3)\\
&r_{\mathrm{v}} = \frac{\beta_{\mathrm{v}}}{\alpha_{\mathrm{v}}}, \quad r_{\mathrm{ev}} = \frac{\beta_{\mathrm{ev}}}{\alpha_{\mathrm{v}}}, \quad r_{\mathrm{a}} = \frac{\beta_{\mathrm{a}}}{2(1+v_{\mathrm{a}})\alpha_{\mathrm{a}}}, \quad r_{\mathrm{ea}} = \frac{\beta_{\mathrm{a}}}{\alpha_{\mathrm{a}}}, \quad k_t = \frac{1}{L^2}\sqrt{\frac{E_2h_2^2}{12\rho_2}} = \sqrt{\frac{\alpha_2^3}{12m_2}}\\
&\alpha_{\mathrm{v}} = \varphi_{\mathrm{v}}\alpha_2, \quad \beta_2 = 1, \quad \varphi_2 = 1, \quad p_{\mathrm{v}1} = \frac{\varphi_1+\varphi_{\mathrm{v}}}{2}, \quad p_{\mathrm{v}2} = \frac{\varphi_2+\varphi_{\mathrm{v}}}{2}, \quad p_{\mathrm{v}3} = \frac{\varphi_{\mathrm{v}}\widetilde{G}_1}{2}, \quad p_{\mathrm{v}4} = \frac{\varphi_{\mathrm{v}}\widetilde{G}_2}{2}\\
&p_{\mathrm{a}1} = \frac{\varphi_2+\varphi_{\mathrm{a}}}{2}, \quad p_{\mathrm{a}2} = \frac{\varphi_3+\varphi_{\mathrm{a}}}{2}, \quad p_{\mathrm{a}3} = \frac{\varphi_{\mathrm{a}}\widetilde{G}_2}{2}, \quad p_{\mathrm{a}4} = \frac{\varphi_{\mathrm{a}}\widetilde{G}_3}{2}
\end{aligned}
\tag{13}
$$

Eq. (12) gives the nondimensional equations of the beam bonded with an ACLD patch, on which only the electric load $\widetilde{V}(\tilde{t})$ is applied. The voltage $\widetilde{V}(\tilde{t})$ can be designed according to proper control laws in order to perform the active vibration control of the composite beams.

2.3. Active control scheme

Since the transverse displacement of each piezoelectric actuator patch is not equal to that of the host beam due to the small stiffness of the VEM layer, the active control may become more difficult. Therefore, the following modal control method can be employed to perform active control of the beam with ACLD patches.

To perform modal control of the beam, the modal velocities for the target modes should be observed first from the charge outputs of the sensor patches. To this end, we design the modal velocity observer (MVO) for the nth target mode as follows:

$$
\begin{aligned}
&y_{n,tt}(t) + 2\omega_{\mathrm{c}n}\zeta_{1n}y_{n,tt}(t) + \omega_{\mathrm{c}n}^2y_n(t) = \omega_{\mathrm{c}n}^2q(t) \qquad z_{n,tt}(t) + 2\omega_{\mathrm{c}n}\zeta_{2n}z_{n,t}(t) + \omega_{\mathrm{c}n}^2z_n(t) = \omega_{\mathrm{c}n}y_{n,t}(t),\\
&\quad n = 1,2,\ldots,N_{\mathrm{c}}
\end{aligned}
\tag{14}
$$

where $\omega_{\mathrm{c}n}$ is the natural frequency of the observer, ζ_{1n} and ζ_{2n} are the damping ratios which can be adjusted to make the closed-loop control more robust, and N_{c} is the number of the modes to be controlled. The output $z_n(t)$ of the observer is 180° out of phase with the target modal velocity when its frequency $\omega_{\mathrm{c}n}$ is equal to that of the target mode.

In order to actively control the N_{c} modes of the beam, the control voltage can be designed based on the observed modal velocities by the N_{c} MVOs

$$
V(t) = \sum_{n=1}^{N_{\mathrm{c}}} g_nz_n(t). \tag{15}
$$

where g_n is the control gain for the nth mode. Eqs. (14) and (15) give a practical control scheme, which is called MVO controller.

The charge output of the sensor and the control voltage can also be nondimensionalized. The nondimensional charge output of the nth sensor patch can be obtained from Eq. (9) as

$$
\tilde{q}(\tilde{t}) = \frac{q(t)}{be_{313}h_2} = \tilde{u}_3(\xi_{\mathrm{r}}) - \tilde{u}_3(\xi_{\mathrm{l}}) \tag{16}
$$

where ξ_{l} and ξ_{r} are the nondimensional co-ordinates at the left and right ends of the piezoelectric sensor patch, respectively.

The nondimensional control voltages applied on the piezoelectric actuator

$$
\widetilde{V}(\tilde{t}) = \sum_{n=1}^{N_{\mathrm{c}}} \tilde{g}_n\tilde{z}_n(\tilde{t}) \tag{17}
$$

where $\tilde{z}_n(\tilde{t})$ is the output of the nth MVO to the nondimensional charge $\tilde{q}(\tilde{t})$, and $\tilde{g}_n$ are the nondimensional control gains given by

$$\tilde{g}_n = \frac{g_n b e_{311} e_{313}}{E_2} \tag{18}$$

Substituting Eq. (17) into Eq. (12), the motion equations of the closed-loop system can be obtained.

3. Control stability analysis and solution scheme

To analyze the effect of the ACLD patch debonding on the control stability of the beam, taking Laplace transformation to Eq. (12), and denoting $\mathbf{Y}_1(\xi) = (\bar{u}_1, \bar{T}_1^e, \bar{w}_1, \psi_1, \bar{Q}_1, \bar{M}_1)^{\mathrm{T}}$, $\mathbf{Y}_2(\xi) = (\bar{u}_2, \bar{T}_2, \bar{w}_2, \psi_2, \bar{Q}_2, \bar{M}_2)^{\mathrm{T}}$, $\mathbf{Y}_3(\xi) = (\bar{u}_3, \bar{T}_3, \bar{w}_3, \psi_3, \bar{Q}_3, \bar{M}_3)^{\mathrm{T}}$ and $\mathbf{Y} = (\mathbf{Y}_1^{\mathrm{T}}, \mathbf{Y}_2^{\mathrm{T}}, \mathbf{Y}_3^{\mathrm{T}})^{\mathrm{T}}$ in which $\bar{T}_1^e = \bar{T}_1 + \bar{V}(\tilde{s})$, the nondimensionalized equation (12) can be written into the following compact form

$$\mathbf{Y}_{,\xi} = \mathbf{A}(k_{\mathrm{v}}, \tilde{s})\mathbf{Y} \quad \xi_1 \leqslant \xi \leqslant \xi_{\mathrm{r}} \tag{19}$$

In Eq. (19), the overbar on the elements of $\boldsymbol{Y}$ stands for the Lapalace transformation, for example,

$$\bar{u}_1(\xi, \tilde{s}) = \int_0^\infty \tilde{u}_1(\xi, \tilde{t}) \mathrm{e}^{-\tilde{s}\tilde{t}} \, \mathrm{d}\tilde{t} \tag{20}$$

and $\mathbf{A}(\tilde{s}) \in C^{18\times 18}$ is a matrix, in terms of complex parameter $\tilde{s}$, which can be expressed as

$$\mathbf{A}(k_{\mathrm{v}}, \tilde{s}) = \begin{bmatrix} \mathbf{A}_{11} & \mathbf{A}_{12} & \mathbf{0} \\ \mathbf{A}_{21} & \mathbf{A}_{22} & \mathbf{A}_{23} \\ \mathbf{0} & \mathbf{A}_{32} & \mathbf{A}_{33} \end{bmatrix} \tag{21}$$

with

$$\mathbf{A}_{11}(\tilde{s}) = \begin{bmatrix} 0 & 1/\widetilde{A}_1 & 0 & 0 & 0 & 0 \\ m_1 s^2 + k_{\mathrm{v}} G_{\mathrm{v}}^* & 0 & 0 & k_{\mathrm{v}} G_{\mathrm{v}}^* p_{\mathrm{v}1} & -k_{\mathrm{v}} G_{\mathrm{v}}^* p_{\mathrm{v}3} & 0 \\ 0 & 0 & 0 & -1/\alpha_2 & \widetilde{G}_1/\alpha_2 & 0 \\ 0 & 0 & 0 & 0 & 0 & 1/\widetilde{D}_1 \\ 0 & 0 & m_1 s^2 + k_{\mathrm{v}} E_{\mathrm{v}}^* & 0 & 0 & 0 \\ k_{\mathrm{v}} r_{t1} G_{\mathrm{v}}^* & 0 & 0 & I_1 s^2 + k_{\mathrm{v}} r_{t1} G_{\mathrm{v}}^* p_{\mathrm{v}1} & r_{q1} - k_{\mathrm{v}} r_{t1} G_{\mathrm{v}}^* p_{\mathrm{v}3} & 0 \end{bmatrix}$$

$$\mathbf{A}_{12}(\tilde{s}) = \begin{bmatrix} 0 & 0 & 0 & 0 & 0 & 0 \\ -k_{\mathrm{v}} G_{\mathrm{v}}^* & 0 & 0 & k_{\mathrm{v}} G_{\mathrm{v}}^* p_{\mathrm{v}2} & -k_{\mathrm{v}} G_{\mathrm{v}}^* p_{\mathrm{v}4} & 0 \\ 0 & 0 & 0 & 0 & 0 & 0 \\ 0 & 0 & 0 & 0 & 0 & 0 \\ 0 & 0 & -k_{\mathrm{v}} E_{\mathrm{v}}^* & 0 & 0 & 0 \\ -k_{\mathrm{v}} r_{t1} G_{\mathrm{v}}^* & 0 & 0 & k_{\mathrm{v}} r_{t1} G_{\mathrm{v}}^* p_{\mathrm{v}2} & k_{\mathrm{v}} r_{t1} G_{\mathrm{v}}^* p_{\mathrm{v}2} & 0 \end{bmatrix}$$

$$\mathbf{A}_{21} = \begin{bmatrix} 0 & 0 & 0 & 0 & 0 & 0 \\ -k_{\mathrm{v}} G_{\mathrm{v}}^* & 0 & 0 & -k_{\mathrm{v}} G_{\mathrm{v}}^* p_{\mathrm{v}1} & k_{\mathrm{v}} G_{\mathrm{v}}^* p_{\mathrm{v}3} & 0 \\ 0 & 0 & 0 & 0 & 0 & 0 \\ 0 & 0 & 0 & 0 & 0 & 0 \\ 0 & 0 & -k_{\mathrm{v}} E_{\mathrm{v}}^* & 0 & 0 & 0 \\ -k_{\mathrm{v}} r_{t2} G_{\mathrm{v}}^* & 0 & 0 & k_{\mathrm{v}} r_{t2} G_{\mathrm{v}}^* p_{\mathrm{v}1} & -k_{\mathrm{v}} r_{t2} G_{\mathrm{v}}^* p_{\mathrm{v}3} & 0 \end{bmatrix}$$

$$\mathbf{A}_{22}(\tilde{s}) = \begin{bmatrix} 0 & 1/\widetilde{A}_2 & 0 & 0 & 0 & 0 \\ m_2 s^2 + k_v G_v^* + r_a & 0 & 0 & p_{a1} r_a - k_v G_v^* p_{v2} & -k_v G_v^* p_{v3} & 0 \\ 0 & 0 & 0 & -1/\alpha_2 & \widetilde{G}_1/\alpha_2 & 0 \\ 0 & 0 & 0 & 0 & 0 & 1/\widetilde{D}_2 \\ 0 & 0 & m_2 s^2 + k_v E_v^* + r_{ea} & 0 & 0 & 0 \\ r_{t2}(r_a - k_v G_v^*) & 0 & 0 & I_2 s^2 + r_{t2}(k_v G_v^* p_{v2} + p_{a1} r_a) & r_{q2} - r_{t2}(k_v G_v^* p_{v4} + p_{a3} r_a) & 0 \end{bmatrix}$$

$$\mathbf{A}_{23}(\tilde{s}) = \begin{bmatrix} 0 & 0 & 0 & 0 & 0 & 0 \\ -r_a & 0 & 0 & p_{a2} r_a & -p_{a4} r_a & 0 \\ 0 & 0 & 0 & 0 & 0 & 0 \\ 0 & 0 & 0 & 0 & 0 & 0 \\ 0 & 0 & -r_{ea} & 0 & 0 & 0 \\ -r_{t2} r_a & 0 & 0 & r_{t2} r_a p_{a2} & -r_{t2} r_a p_{a4} & 0 \end{bmatrix}$$

$$\mathbf{A}_{32} = \begin{bmatrix} 0 & 0 & 0 & 0 & 0 & 0 \\ -r_a & 0 & 0 & -p_{a1} r_a & p_{a3} r_a & 0 \\ 0 & 0 & 0 & 0 & 0 & 0 \\ 0 & 0 & 0 & 0 & 0 & 0 \\ 0 & 0 & -r_{ea} & 0 & 0 & 0 \\ r_{t3} r_a & 0 & 0 & r_{t3} r_a p_{a1} & -r_{t3} r_a p_{a3} & 0 \end{bmatrix}$$

$$\mathbf{A}_{33}(\tilde{s}) = \begin{bmatrix} 0 & 1/\widetilde{A}_3 & 0 & 0 & 0 & 0 \\ m_3 s^2 + r_a & 0 & 0 & -r_a p_{a2} & r_a p_{a4} & 0 \\ 0 & 0 & 0 & -1/\alpha_2 & \widetilde{G}_3/\alpha_2 & 0 \\ 0 & 0 & 0 & 0 & 0 & 1/\widetilde{D}_3 \\ 0 & 0 & m_3 s^2 + r_{ea} & 0 & 0 & 0 \\ -r_{t3} r_a & 0 & 0 & I_3 s^2 + r_{t3} r_a p_{a2} & r_{q3} - r_{t3} r_a p_{a4} & 0 \end{bmatrix} \tag{22}$$

Note that in Eq. (22) $s = k_t \tilde{s}$, $G_v^*(\tilde{s})$ and $E_v^*(\tilde{s})$ are functions of $\tilde{s}$. Indeed, after taking Laplace transformation, the nondimensional shear and peel stresses of the VEM in Eq. (12) become

$$\begin{aligned} \bar{\tau}_v(\xi, \tilde{s}) &= k_v G_v^*(\tilde{s}) \bar{\gamma}_v(\xi, \tilde{s}) \\ \bar{\sigma}_v(\xi, \tilde{s}) &= k_v E_v^*(\tilde{s}) \bar{\varepsilon}_v(\xi, \tilde{s}) \end{aligned} \tag{23}$$

Employing the Golla–Hughes–McTavish (GHM) model (McTavish and Hughes, 1993), the shear modulus of the VEM in the s-domain has the following form:

$$G_v^*(\tilde{s}) = \frac{G_v^\infty}{E_2 \alpha_v} \left[1 + \sum_{k=1}^{K} \widehat{\alpha}_k \frac{s^2 + 2\widehat{\zeta}_k \widehat{\omega}_k s}{s^2 + 2\widehat{\zeta}\widehat{\omega}_k s + \widehat{\omega}_k^2} \right] \tag{24}$$

where $\widehat{\alpha}_k$, $\widehat{\zeta}_k$ and $\widehat{\omega}_k$ are constants that determine the shape of the modulus in s-domain.

Similarly, the extension modulus can also be expressed as

$$E_v^*(\tilde{s}) = \frac{E_v^\infty}{E_2 \alpha_v} \left[1 + \sum_{k=1}^{K} \breve{\alpha}_k \frac{s^2 + 2\breve{\zeta}_k \breve{\omega}_k s}{s^2 + 2\breve{\zeta}\breve{\omega}_k s + \breve{\omega}_k^2} \right] \tag{25}$$

where $\breve{\alpha}_k$, $\breve{\zeta}_k$ and $\breve{\omega}_k$ are also constants used to determine the modulus.

It should be noted that Eq. (19) is a set of homogeneous equations and the control items related to the voltage appear in the boundary conditions of the piezoelectric actuator patches for uniformly distributed control voltage.

Similarly, the equations of motion of the host beam itself (segment OA and BC) can also be transformed into the following form:

$$\mathbf{Y}_{2,\xi} = \mathbf{A}_2(\tilde{s})\mathbf{Y}_2 \quad 0 \leqslant \xi \leqslant \xi_l, \quad \xi_r \leqslant \xi \leqslant 1 \tag{26}$$

where $\widetilde{\mathbf{A}}_2 \in C^{6\times 6}$ is the state matrix for the host beam as given by

$$\mathbf{A}_2(\tilde{s}) = \begin{bmatrix} 0 & 1/\widetilde{A}_2 & 0 & 0 & 0 & 0 \\ m_2 s^2 & 0 & 0 & 0 & 0 & 0 \\ 0 & 0 & 0 & -1/\alpha_2 & \widetilde{G}_2/\alpha_2 & 0 \\ 0 & 0 & 0 & 0 & 0 & 1/\widetilde{D}_2 \\ 0 & 0 & m_2 s^2 & 0 & 0 & 0 \\ 0 & 0 & 0 & I_2 s^2 & r_{q3} & 0 \end{bmatrix} \tag{27}$$

In addition to the basic equations for different portions of the beam, the continuity conditions at the debonding interface and boundary conditions for the host beam and the piezoelectric patches should also be considered. The continuity condition to guarantee the displacement continuity and force balance at the interface between the perfectly bonded and debonded parts in the ACLD patch can be expressed as

$$\mathbf{Y}(\xi_d^-) = \mathbf{Y}(\xi_d^+) \tag{28}$$

where ξ_d is the nondimensional coordinate of the interface, as shown in Fig. 1. The boundary conditions for the host beam and the piezoelectric actuator and sensor patch can be written as follows:

$$\begin{aligned} &\mathbf{D}_{\mathrm{hl}}\mathbf{Y}_2(0) + \mathbf{D}_{\mathrm{hr}}\mathbf{Y}_2(1) = \mathbf{D}_{\mathrm{h}} \\ &\mathbf{D}_{\mathrm{al}}\mathbf{Y}_1(\xi_l) + \mathbf{D}_{\mathrm{ar}}\mathbf{Y}_1(\xi_r) = \mathbf{D}_{\mathrm{a}} \\ &\mathbf{D}_{\mathrm{sl}}\mathbf{Y}_3(\xi_l) + \mathbf{D}_{\mathrm{sr}}\mathbf{Y}_3(\xi_r) = \mathbf{D}_{\mathrm{s}} \end{aligned} \tag{29}$$

where $\mathbf{D}_{\mathrm{hl}}$, $\mathbf{D}_{\mathrm{al}}$, $\mathbf{D}_{\mathrm{sl}}$, $\mathbf{D}_{\mathrm{hr}}$, $\mathbf{D}_{\mathrm{ar}}$ and $\mathbf{D}_{\mathrm{sr}}$ are 6×6 matrices, $\mathbf{D}_{\mathrm{h}}$, $\mathbf{D}_{\mathrm{a}}$ and $\mathbf{D}_{\mathrm{s}}$ are known vectors corresponding to the given boundary conditions of the host beam, actuator and sensor patches, respectively. When the boundary conditions are homogeneous for the host beam and the sensor patches, $\mathbf{D}_{\mathrm{h}} = \mathbf{D}_{\mathrm{s}} = 0$. In general, the boundary condition of the piezoelectric actuator patch is not homogeneous due to the applied control voltage. For instance, for a free–free piezoelectric actuator patch, the boundary condition has the form

$$\begin{bmatrix} 0 & 1 & 0 & 0 & 0 & 0 \\ 0 & 0 & 0 & 0 & 1 & 0 \\ 0 & 0 & 0 & 0 & 0 & 1 \\ 0 & 0 & 0 & 0 & 0 & 0 \\ 0 & 0 & 0 & 0 & 0 & 0 \\ 0 & 0 & 0 & 0 & 0 & 0 \end{bmatrix} \begin{Bmatrix} \bar{u}_1(\xi_l) \\ \bar{T}_1^e(\xi_l) \\ \bar{w}_1(\xi_l) \\ \bar{\psi}_1(\xi_l) \\ \bar{Q}_1(\xi_l) \\ \bar{M}_1(\xi_l) \end{Bmatrix} + \begin{bmatrix} 0 & 0 & 0 & 0 & 0 & 0 \\ 0 & 0 & 0 & 0 & 0 & 0 \\ 0 & 0 & 0 & 0 & 0 & 0 \\ 0 & 1 & 0 & 0 & 0 & 0 \\ 0 & 0 & 0 & 0 & 1 & 0 \\ 0 & 0 & 0 & 0 & 0 & 1 \end{bmatrix} \begin{Bmatrix} \bar{u}_1(\xi_r) \\ \bar{T}_1^e(\xi_r) \\ \bar{w}_1(\xi_r) \\ \bar{\psi}_1(\xi_r) \\ \bar{Q}_1(\xi_r) \\ \bar{M}_1(\xi_r) \end{Bmatrix} = \begin{bmatrix} 1 \\ 0 \\ 0 \\ 1 \\ 0 \\ 0 \end{bmatrix} \bar{V}(\tilde{s}) \tag{30}$$

where $\bar{V}(\tilde{s})$ is the Laplace transformation of the nondimensioanal control voltage $\widetilde{V}(\tilde{t})$. Taking Laplace transformation to Eqs. (14), (16) and (17), yields

$$\bar{V}(\tilde{s}) = \bar{q}(\tilde{s}) \sum_{n=1}^{N_c} g_n H_n(\tilde{s}) = [\bar{u}_3(\xi_r, \tilde{s}) - \bar{u}_3(\xi_l, \tilde{s})] \sum_{n=1}^{N_c} g_n H_n(\tilde{s}) \tag{31}$$

where $H_n(\tilde{s})$is the transfer function of the nth modal velocity observer given by

$$H_n(\tilde{s}) = \frac{\omega_{cn}^3 s}{(s^2 + 2\omega_{cn}\zeta_{1n}s + \omega_{cn}^2)(s^2 + 2\omega_{cn}\zeta_{2n}s + \omega_{cn}^2)} \tag{32}$$

Substituting Eq. (31) into Eq. (30), gives

$$\mathbf{D}_{\mathrm{al}}\mathbf{Y}_1(\xi_{\mathrm{l}}) + \mathbf{D}_{\mathrm{ar}}\mathbf{Y}_1(\xi_{\mathrm{r}}) + \mathbf{D}_{\mathrm{cl}}\mathbf{Y}_3(\xi_{\mathrm{l}}) + \mathbf{D}_{\mathrm{cr}}\mathbf{Y}_3(\xi_{\mathrm{r}}) = \mathbf{0} \tag{33}$$

where

$$\mathbf{D}_{\mathrm{cl}} = \begin{bmatrix} \sum_{n=1}^{N_{\mathrm{c}}} g_n H_n(\tilde{s}) & 0 & 0 & 0 & 0 & 0 \\ 0 & 0 & 0 & 0 & 0 & 0 \\ 0 & 0 & 0 & 0 & 0 & 0 \\ \sum_{n=1}^{N_{\mathrm{c}}} g_n H_n(\tilde{s}) & 0 & 0 & 0 & 0 & 0 \\ 0 & 0 & 0 & 0 & 0 & 0 \\ 0 & 0 & 0 & 0 & 0 & 0 \end{bmatrix}; \quad \mathbf{D}_{\mathrm{cr}} = \begin{bmatrix} -\sum_{n=1}^{N_{\mathrm{c}}} g_n H_n(\tilde{s}) & 0 & 0 & 0 & 0 & 0 \\ 0 & 0 & 0 & 0 & 0 & 0 \\ 0 & 0 & 0 & 0 & 0 & 0 \\ -\sum_{n=1}^{N_{\mathrm{c}}} g_n H_n(\tilde{s}) & 0 & 0 & 0 & 0 & 0 \\ 0 & 0 & 0 & 0 & 0 & 0 \\ 0 & 0 & 0 & 0 & 0 & 0 \end{bmatrix} \tag{34}$$

The boundary conditions in Eq. (33) give the relationship between the actuator and the sensor patches, which depends on the control law.

To investigate the debonding of the ACLD patch on both passive and hybrid control of the beam, an effective way is to examine the eigenvalues of the beam, which give many useful information such as modal frequencies, modal damping ratios. More importantly, the eigenvalues of the beam can be used to judge the control stability and the degree of stability of the controlled system. The characteristic equation of the beam with a partly debonded ACLD patch can be derived as follows.

After taking Laplace transformation, the partial differential equations of motion of the beam with and without ACLD patch become a set of ordinary differential equations as given in Eqs. (19) and (26). For different portions, the solutions of these equations can be written as follows:

$$\begin{aligned} &\bar{\mathbf{Y}}_2(\xi_{\mathrm{l}}) = \mathbf{\Phi}_{\mathrm{OA}}(\tilde{s})\bar{\mathbf{Y}}_2(0) \quad 0 < \xi < \xi_{\mathrm{l}} \\ &\bar{\mathbf{Y}}(\xi_d^-) = \mathbf{\Phi}_{\mathrm{AD}}(\tilde{s})\bar{\mathbf{Y}}(\xi_A) \quad \xi_A < \xi < \xi_d^- \\ &\bar{\mathbf{Y}}(\xi_{\mathrm{r}}) = \mathbf{\Phi}_{\mathrm{DB}}(\tilde{s})\bar{\mathbf{Y}}(\xi_d^+) \quad \xi_d^+ < \xi < \xi_{\mathrm{r}} \\ &\bar{\mathbf{Y}}_2(1) = \mathbf{\Phi}_{\mathrm{BC}}(\tilde{s})\bar{\mathbf{Y}}_2(\xi_{\mathrm{r}}) \quad \xi_{\mathrm{r}} < \xi < 1 \end{aligned} \tag{35}$$

where $\mathbf{\Phi}_{\mathrm{OA}} \in R^{6\times 6}$, $\mathbf{\Phi}_{\mathrm{AD}} \in R^{18\times 18}$, $\mathbf{\Phi}_{\mathrm{DB}} \in R^{18\times 18}$ and $\mathbf{\Phi}_{\mathrm{BC}} \in R^{6\times 6}$ are transition matrices given by

$$\begin{aligned} &\mathbf{\Phi}_{\mathrm{OA}}(\tilde{s}) = \mathrm{e}^{\mathbf{A}_2(\tilde{s})\xi_l}, \quad \mathbf{\Phi}_{\mathrm{BC}}(\tilde{s}) = \mathrm{e}^{\mathbf{A}_2(\tilde{s})(1-\xi_r)} \\ &\mathbf{\Phi}_{\mathrm{AD}}(\tilde{s}) = \mathrm{e}^{\mathbf{A}(0,\tilde{s})(\xi_d-\xi_{\mathrm{l}})}, \quad \mathbf{\Phi}_{\mathrm{AD}}(\tilde{s}) = \mathrm{e}^{\mathbf{A}(1,\tilde{s})(\xi_{\mathrm{r}}-\xi_d)} \end{aligned} \tag{36}$$

By adding following continuity and homogeneous boundary conditions

$$\begin{aligned} &\mathbf{Y}_2(\xi_{\mathrm{l}}) = [\mathbf{0}_6 \quad \mathbf{I}_6 \quad \mathbf{0}_6]\,\mathbf{Y}(\xi_l) \quad \text{at } \xi = \xi_A \\ &\mathbf{Y}(\xi_d^-) = \mathbf{Y}(\xi_d^+) \quad \text{at } \xi = \xi_d \\ &\mathbf{Y}_2(\xi_{\mathrm{r}}) = [\mathbf{0}_6 \quad \mathbf{I}_6 \quad \mathbf{0}_6]\,\mathbf{Y}(\xi_B) \quad \text{at } \xi = \xi_B \\ &\mathbf{D}_{\mathrm{al}}\mathbf{Y}_1(\xi_{\mathrm{l}}) + \mathbf{D}_{\mathrm{ar}}\mathbf{Y}_1(\xi_{\mathrm{r}}) + \mathbf{D}_{\mathrm{cl}}\mathbf{Y}_3(\xi_{\mathrm{l}}) + \mathbf{D}_{\mathrm{cr}}\mathbf{Y}_3(\xi_{\mathrm{r}}) = 0 \quad \text{for actuator} \\ &\mathbf{D}_{\mathrm{sl}}\mathbf{Y}_3(\xi_{\mathrm{l}}) + \mathbf{D}_{\mathrm{sr}}\mathbf{Y}_3(\xi_{\mathrm{r}}) = 0 \quad \text{for sensor} \\ &\mathbf{D}_{\mathrm{hl}}\mathbf{Y}_2(0) + \mathbf{D}_{\mathrm{hr}}\mathbf{Y}_2(1) = 0 \quad \text{for host beam} \end{aligned} \tag{37}$$

and denoting $\mathbf{Z} = [\mathbf{Y}_2^{\mathrm{T}}(0), \mathbf{Y}_2^{\mathrm{T}}(\xi_l), \mathbf{Y}^{\mathrm{T}}(\xi_{\mathrm{l}}), \mathbf{Y}^{\mathrm{T}}(\xi_d^-), \mathbf{Y}^{\mathrm{T}}(\xi_d^+), \mathbf{Y}^{\mathrm{T}}(\xi_{\mathrm{r}}), \mathbf{Y}_2^{\mathrm{T}}(\xi_{\mathrm{r}}), \mathbf{Y}_2^{\mathrm{T}}(1)]^{\mathrm{T}}$, Eq. (37) together with the continuity and boundary conditions can be written into the following compact form

$$\mathbf{R}(\tilde{s})\mathbf{Z} = \mathbf{0} \tag{38}$$

where

$$\mathbf{R}(\tilde{s}) = \begin{bmatrix} \mathbf{\Phi}_{OA} & -\mathbf{I}_6 & & \mathbf{0} & & \mathbf{0} & \mathbf{0} & & \mathbf{0} & & \mathbf{0} & \mathbf{0} \\ \mathbf{0} & \mathbf{I}_6 & [\mathbf{0}_6 & -\mathbf{I}_6 & \mathbf{0}_6] & \mathbf{0} & \mathbf{0} & & \mathbf{0} & & \mathbf{0} & \mathbf{0} \\ \mathbf{0} & \mathbf{0} & & \mathbf{\Phi}_{Ad} & & -\mathbf{I}_{18} & \mathbf{0} & & \mathbf{0} & & \mathbf{0} & \mathbf{0} \\ \mathbf{0} & \mathbf{0} & & \mathbf{0} & & \mathbf{I}_{18} & -\mathbf{I}_{18} & & \mathbf{0} & & \mathbf{0} & \mathbf{0} \\ \mathbf{0} & \mathbf{0} & & \mathbf{0} & & \mathbf{0} & \mathbf{\Phi}_{dB} & & -\mathbf{I}_{18} & & \mathbf{0} & \mathbf{0} \\ \mathbf{0} & \mathbf{0} & & \mathbf{0} & & \mathbf{0} & \mathbf{0} & [\mathbf{0}_6 & \mathbf{I}_6 & \mathbf{0}_6] & -\mathbf{I}_6 & \mathbf{0} \\ \mathbf{0} & \mathbf{0} & & \mathbf{0} & & \mathbf{0} & \mathbf{0} & & \mathbf{0} & & \mathbf{\Phi}_{BC} & -\mathbf{I}_6 \\ \mathbf{0} & \mathbf{0} & [\mathbf{D}_{al} & \mathbf{0}_6 & \mathbf{D}_{cl}] & \mathbf{0} & \mathbf{0} & [\mathbf{D}_{ar} & \mathbf{0}_6 & \mathbf{D}_{cr}] & \mathbf{0} & \mathbf{0} \\ \mathbf{0} & \mathbf{0} & [\mathbf{0}_6 & \mathbf{0}_6 & \mathbf{D}_{cl}] & \mathbf{0} & \mathbf{0} & [\mathbf{0}_6 & \mathbf{0}_6 & \mathbf{D}_{cl}] & \mathbf{0} & \mathbf{0} \\ \mathbf{D}_{hl} & \mathbf{0} & & \mathbf{0} & & \mathbf{0} & \mathbf{0} & & \mathbf{0} & & \mathbf{0} & \mathbf{D}_{hr} \end{bmatrix} \tag{39}$$

Eq. (38) has a nontrivial solution only when

$$\det[\mathbf{R}(\tilde{s})] = 0 \tag{40}$$

Eq. (40) is an algebraic equation of the complex eigenvalue $\tilde{s}$, from which the eigenvalues of the beam with debonded ACLD patches can be solved. When computing the eigenvalues, the ACLD patch should be divided into several small segments in order to obtain the eigenvalues with higher precision. Each complex eigenvalue gives the information of active damping and frequency for each vibration mode. For instance, the real part of an eigenvalue $\tilde{s}$ is proportional to the damping ratio of a mode, and its imaginary part is the nondimensional damped modal frequency. Most importantly, the eigenvalues can be used for a control stability analysis by examining the signs of their real parts. If all the eigenvalues have negative real parts, the controlled beam is asymptotically stable.

4. Comparison with other models

In the present model, not only the incompatibility of the transverse displacement in the constraining layer and the host structure, but also their inertia and shear effects are considered. In addition, the adhesive layer between the host structure and the piezoelectric layer is also modeled. To validate the proposed model, comparisons with the results from literatures are given in this section.

An example of a cantilever beam treated with an ACLD patch but without a piezoelectric sensor patch based on an existing model can be found in Shi et al. (2001), as shown in Fig. 2. Using the finite element method (FEM) (the total element number is 10) and one term GHM model of the VEM, Shi et al. (2001) calculated the first five eigenvalues of a beam whose dimensional and physical properties are given in Table 1. The real and imaginary parts of the first five eigenvalues given in Shi et al. (2001) are listed in Table 2.

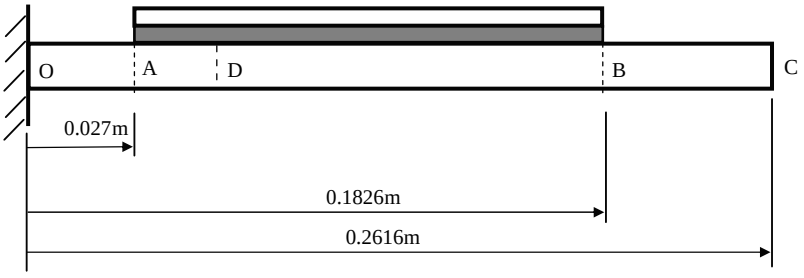

Fig. 2. Beam treated with an ACLD patch (without sensor patch).

Table 1
Material properties and geometrical dimensions

L	0.2616 m	h_2	0.002286 m	E_1	74×10^9Pa	$\hat{\xi}$	4.0
x_l	0.027 m	h_v	0.00025 m	E_2	71×10^9Pa		
x_r	0.1286 m	ρ_l	7600 kg/m^3	G_v^∞	5×10^5Pa		
b	0.0127 m	ρ_2	2700 kg/m^3	α	6.0		
h_1	0.000762 m	ρ_v	1250 kg/m^3	$\hat{\omega}$	10000 rad/s		

Table 2
The first five eigenvalues obtained by the present model and that given in Shi et al. (2001)

Mode no.	Present model					
	Timosenko's theory		Euler's theory		FEA result (Shi et al., 2001)	
	Real	Imaginary	Real	Imaginary	Real	Imaginary
1	−1.900	±174.467	−1.900	±174.478	−2.2424	±175.124
2	−11.557	±938.020	−11.561	±938.375	−13.006	±944.466
3	−37.713	±2747.575	−37.769	±2750.087	−39.206	±2776.994
4	−22.788	±5116.646	−22.858	±5125.073	−24.368	±5207.037
5	−22.817	±8666.016	−22.856	±8686.915	−22.105	±8932.071

For the purpose of comparison, the first five complex eigenvalues are also calculated using the present model. In the computation, in addition to the parameters as given in Table 1, the Poisson's ratios for the piezoelectric and the host beam are taken as $\mu_1 = \mu_2 = 0.3$ to determine the shear modulus. Moreover, the Young's modulus E_v of the VEM is simply assumed to be $G_v^\infty/(2(1+\mu_v))$ and μ_v is taken as 0.4. The results of the first five eigenvalues obtained by present model are listed in Table 2. To examine the effects of the shear and inertia of the beam, the results obtained by employing the Euler–Bernoulli beam theory are also given in Table 2.

Table 2 shows that the frequencies (imaginary parts of the eigenvalues) obtained by Timoshenko's beam theory are lower than those by Euler–Bernoulli beam theory particularly for the higher order modes. However, no noticeable differences in the damping coefficients (the absolute values of the real parts of the eigenvalues) obtained by the two theories are observed due to the small thickness-to-length ratio in this example.

It can be found from Table 2 that all the five frequencies obtained by using the present model are smaller than the corresponding ones from the results given in Shi et al. (2001) because of the consideration of the compressional vibration in the VEM in the present model. In other words, when the compressional vibration in the soft VEM is modeled, the equivalent bending stiffness of the entire composite beam becomes smaller. The relative differences for the first five frequencies are 0.38%, 0.68%, 1.06%, 1.74% and 2.98%. Table 2 also shows that the first four damping coefficients calculated using the present model are also smaller than those by Shi et al. (2001) and the relative differences between them are 15.27%, 11.14%, 3.81% and 6.48%, respectively. One the contrary, the damping coefficients for the fifth mode obtained by the present model is larger than the corresponding result given in Shi et al. (2001) and the relative difference for the fifth mode is 3.22%. This is because the higher order modes are more sensitive to the compressional vibration. Another reason for this may be that the eigenvalues corresponding to the higher order modes obtained by FEM is not accurate if the element number is small (Lee and Kim, 2001). Lee and Kim (2001) show that the modal damping for higher order modes of a beam fully treated with an ACLD layer calculated by FEM become larger as the element number increases.

Another example of a beam with fully covered ACLD layer can be found in (Lee and Kim, 2001) in which the same parameters are used except the Young's modulus of the piezoelectric layer is 64.9 GPa

Table 3
Comparison of passive damping ratios obtained by the present model and the spectral element method (Lee and Kim, 2001)

Mode no.	Present model		Spectral element model (Lee and Kim, 2001)	Relative differences
	Eigenvalues	Damping ratios	Damping ratios	
1	-9.154 ± 171.184I	0.0534	0.0589	9.34%
2	-75.327 ± 980.170I	0.0766	0.0830	7.71%
3	-96.187 ± 2590.600I	0.0371	0.0403	7.94%
4	-83.624 ± 4785.97I	0.0175	0.0192	8.85%
5	-64.877 ± 7583.3I	0.00855	0.0095	10%

instead of 74 GPa. Using a spectral finite element model in which all layers are assumed to have the same transverse displacement, the passive damping ratios for the first five modes are given in Table 3. The first five eigenvalues and the corresponding damping ratios obtained by the present model are also listed in Table 3.

It can be seen from Table 3 that the damping ratios obtained using the current model are smaller than those of the models in which no compressional vibration is modeled. Their relative differences range from 7.7% to 10%, as tabulated in Table 2. This is because the compressional vibration of the VEM decreases its shear strain and consequently weakens its passive damping effect.

In summary, due to the consideration of the compressional vibration of the VEM in the present model, both the passive damping ratios and the modal frequencies obtained by the present model are smaller than those obtained by the existing models. For a thicker VEM, the differences may become even larger.

5. Example and analysis

As an illustrative example, consider a cantilevered beam treated with an ACLD patch, as shown in Fig. 1. The nondimensional length of the ACLD patch is 0.39 and the nondimensional distance from the clamped end of the beam to the left end of the ACLD patch is 0.103. The physical parameters used in the example are $v_1 = v_2 = v_3 = 0.3$, $v_v = 0.4$, $v_a = 0.34$, $\alpha_2 = 0.0087$, $\beta_1 = 1.04$, $\beta_3 = 0.986$, $\eta_1 = \eta_3 = 7.33 \times 10^{-9}$, $\eta_2 = 2.6 \times 10^{-9}$, $\beta_v(s) = 7.04 \times 10^{-6}\left(1 + 6\frac{s^2+80000s}{s^2+80000s+10^8}\right)$, $\beta_{ev} = 1.97 \times 10^{-5}$, $\beta_a = 0.01$, $\beta_{ea} = 0.028$, $\varphi_1 = 0.333$, $\varphi_3 = 0.131$, $\varphi_v = 0.11$, $\varphi_a = 0.066$.

For the beam with perfectly bonded ACLD patch, the first eight eigenvalues of the open-loop system are calculated and listed in Table 4. It is shown that all the real parts of these eigenvalues are negative due to the

Table 4
The first eight eigenvalues of beam with perfectly bonded ACLD patch

Mode no.	Open-loop	Closed-loop	
		MVO controller	PD controller
1	$-0.020 + 4.329I$	$-0.424 + 4.0224I$	$-0.022 + 4.327I$
2	$-0.118 + 20.744I$	$-0.580 + 20.508I$	$-0.205 + 20.696I$
3	$-0.685 + 65.919I$	$-1.649 + 65.540I$	$-5.154 + 64.328I$
4	$-0.354 + 120.501I$	$-0.580 + 120.618I$	$-3.892 + 118.640I$
5	$-0.306 + 207.930I$	$-0.295 + 207.976I$	$-3.270 + 206.082I$
6	$-0.305 + 294.962I$	$-0.283 + 294.989I$	$-6.307 + 288.883I$
7	$-0.216 + 412.81I$	$-0.217 + 412.809I$	$\mathbf{0.318 + 413.622I}$
8	$-0.181 + 503.342I$	$-0.181 + 503.342I$	$-0.202 + 503.293I$

passive damping effect of the constrained VEM. The damping effect of the ACLD can be significantly enhanced by the active control.

5.1. Comparison between MVO and PD controller

In active control, the proportional plus derivative (PD) controller is widely used and the control voltage is designed as

$$\widetilde{V}(\tilde{t}) = -g_p\tilde{\boldsymbol{q}}(\tilde{t}) - g_d\dot{\tilde{\boldsymbol{q}}}(\tilde{t})$$

where g_p and g_d are the nondimensional control gains. When $g_p = 0$ and $g_d = 7.4 \times 10^{-4}$, the eigenvalues of the controlled beam are presented in Table 4. It can be seen that the active damping are added to the first six modes by the active control. The PD controller cannot concentrate the control energy properly to the target modes. For example, the active control adds only small active damping to the dominant mode 1 and mode 2, whereas it produces relatively larger active damping to mode 3 to mode 6. In addition, the seventh mode becomes unstable since the corresponding eigenvalue has a positive real part caused by the PD control. The reason for the destabilization of the higher modes is that the actuator and the sensor do not undergo the identical vibration due to the soft VEM between the actuator and the host beam. Therefore, the information related to the modes with higher order should be removed from the sensed signal to keep the entire control system stable.

Since the MVO functions as a band-pass filter, the MVO controller can be used to perform modal control of the designated modes without remarkably affecting the residual modes. In order to control the first four modes, according to the control law in Eq. (14), the nondimensional control gains are taken as 0.3, 0.09, 0.015 and 0.006, respectively. The damping ratios in the observers in Eq. (14) for these controlled modes are 0.5 and 0.6, respectively, and the four frequencies of the open-loop beam, 4.329, 20.744, 65.919 and 120.501, are taken as the natural frequencies of the four observers. For the beam with perfectly bonded ACLD patch controlled by the MVOs, the first eight eigenvalues are also obtained and given in Table 4. As shown in Table 4, the first four modes are effectively controlled and the residual modes are not affected by the active control and they still remain stable. Unlike the PD controller, the control gains in the MVO controller can be selected independently so that the control energy can be distributed properly among the controlled modes. Compared to the PD controller, the MVO controller is more robust and is to be used in the following discussion.

5.2. Effect of debonding

To examine the effects of the ACLD debonding on the passive and hybrid control, an edge debonding between the actuator and the host beam at the left end of the ACLD patch is introduced. When the debonding length is taken as 5%, 10%, 15%, 20%, 25% and 30% of the entire ACLD patch, respectively, the first five eigenvalues of both the passively and hybridly controlled beam are calculated and given in Table 5. Since the debonded part of the piezoelectric actuator can also vibrate in a way approximately similar to a small cantilever beam, additional modes are induced, and the eigenvalues for the additional modes are also listed in Table 5.

First, we check the effects of the edge debonding of the ACLD patch on frequencies. Fig. 3 depicts the frequency changes of the first five frequencies of the passively controlled beam versus the debonding length. It shows that each frequency does not simply decrease as the debonding length increases and exhibits a complicated trend dependent on the debonding length. It is noted from Fig. 3 that the additional modes induced by the edge debonding of the ACLD patch can significantly affect the modal frequencies of the composite beam, which can be observed clearly from the relative frequency change shown in Fig. 4. When the debonding is in such a small range that the frequencies of the induced additional modes are very high

Table 5
The effect of debonding on the eigenvalues of open- and closed-loop system

Debonding length (%)	Open-loop	Closed-loop
0	$-0.020 + 4.329I$	$-0.424 + 4.0224I$
	$-0.118 + 20.744I$	$-0.580 + 20.508I$
	$-0.685 + 65.919I$	$-1.649 + 65.540I$
	$-0.354 + 120.501I$	$-0.580 + 120.618I$
	$-0.306 + 207.930I$	$-0.295 + 207.976I$
5	$-0.016 + 4.323I$	$-0.296 + 4.116I$
	$-0.117 + 20.740I$	$-0.540 + 20.503I$
	$-0.639 + 65.621I$	$-1.482 + 65.225I$
	$-0.275 + 119.727I$	$-0.443 + 119.810I$
	$-0.284 + 205.632I$	$-0.270 + 205.699I$
10	$-0.013 + 4.318I$	$-0.221 + 4.161I$
	$-0.114 + 20.732I$	$-0.495 + 20.504I$
	$-0.576 + 65.199I$	$-1.294 + 64.835I$
	$-0.151 + 117.301I$	$-0.238 + 117.340I$
	$-0.304 + 164.085I$[a]	$-0.340 + 164.203I$[a]
	$-0.256 + 217.768I$	$-0.256 + 217.882I$
15	$-0.011 + 4.314I$	$-0.168 + 4.191I$
	$-0.110 + 20.719I$	$-0.446 + 20.506I$
	$-0.478 + 64.394I$	$-1.047 + 64.069I$
	$-0.097 + 96.159I$[a]	$-0.097 + 96.158I$[a]
	$-0.306 + 126.064I$	$-0.459 + 126.165I$
	$-0.245 + 214.413I$	$-0.236 + 214.447I$
20	$-0.008 + 4.311I$	$-0.129 + 4.214I$
	$-0.104 + 20.701I$	$-0.394 + 20.505I$
	$-0.161 + 59.948I$[a]	$-0.333 + 59.807I$[a]
	$-0.390 + 70.825I$	$-0.701 + 70.750I$
	$-0.184 + 122.970I$	$-0.281 + 123.024I$
	$-0.238 + 214.245I$	$-0.227 + 214.283I$
25	$-0.007 + 4.308I$	$-0.099 + 4.232I$
	$-0.095 + 20.674I$	$-0.342 + 20.498I$
	$-0.043 + 45.770I$[a]	$-0.043 + 45.770I$[a]
	$-0.435 + 66.449I$	$-0.879 + 66.274I$
	$-0.117 + 122.341I$	$-0.175 + 122.373I$
	$-0.238 + 213.491I$	$-0.227 + 213.531I$
30	$-0.005 + 4.306I$	$-0.076 + 4.246I$
	$-0.084 + 20.624I$	$-0.289 + 20.468I$
	$-0.042 + 34.695I$[a]	$-0.041 + 34.688I$[a]
	$-0.356 + 65.717I$	$-0.717 + 65.555I$
	$-0.068 + 121.943I$	$-0.097 + 121.958I$
	$-0.220 + 205.090I$	$-0.211 + 205.137I$
	$-0.088 + 234.315I$[a]	$-0.087 + 234.316I$[a]

[a] Indicates the additional modes induced by the debonding of the ACLD patch.

and beyond the considered frequency range, the several lower frequencies of the composite beam decrease with expansion of the debonding. For example, a 5% debonding results in 0.14%, 0.02%, 0.45%, 0.64% and 1.1% of decrease of the first five frequencies, respectively. However, the modal frequencies, which are close to those of the debonding-induced modes, will either increase or decrease noticeably, as shown in Fig. 4 and Table 5. Fig. 3 reveals that the additional modes tend to push their neighbor modes away from themselves.

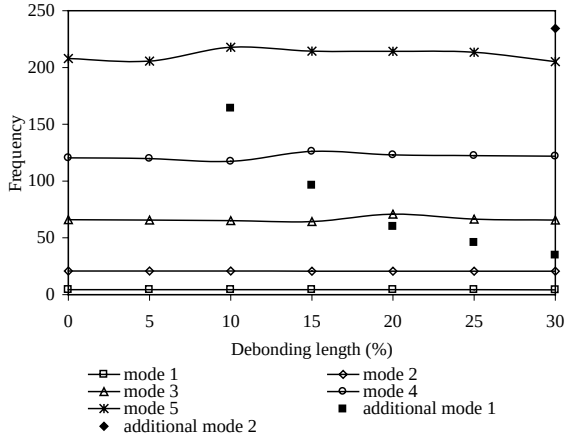

Fig. 3. Frequency changes vs. debonding length.

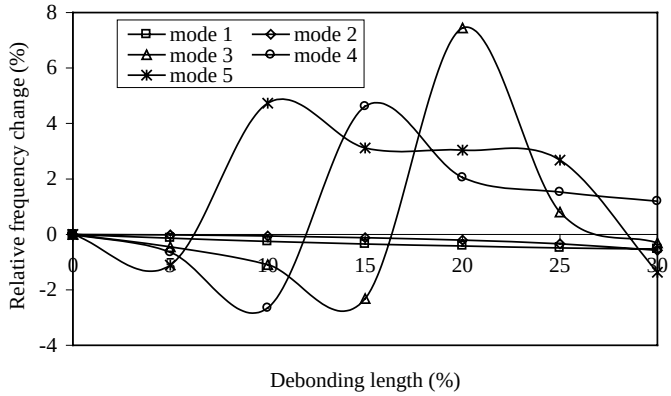

Fig. 4. Relative change of the modal frequencies caused by the debonding.

For instance, when the first additional mode induced by a 10% edge debonding lies between the fourth and fifth modes of the beam, it leads to a 2.7% reduction of the fourth modal frequency but a 4.7% increase of the fifth. In fact, an edge debonding has changed the original structure into a different structure, which has a completely new frequency structure particularly in the higher frequency range.

Second, the effects of the edge debonding on the passive control of the beam are investigated. The obtained damping ratios from the eigenvalues for different debonding length are plotted in Fig. 5. Fig. 5 shows that the debonding can significantly change the passive damping ratios. The passive damping ratios for mode 1, 2, 3 and 5 are reduced by the ACLD debonding. For example, when an 15% debonding occurs at the left end of the ACLD patch, the passive damping ratios for these modes reduced by 44.8%, 6.7%, 28.6% and 22.4%, respectively. The modal damping ratios of mode 1, 2 and 5 decrease as the debonding length increases. However, the trend of damping ratio change is different for mode 3 and mode 4 at some debonding lengths. For example, when the debonding length is 15%, the damping ratio of the fourth mode is much larger than those with other debonding lengths. This means that the additional modes induced by the ACLD debonding affect not only the modal frequencies, but also the modal damping ratios of their neighbor modes of the composite beam.

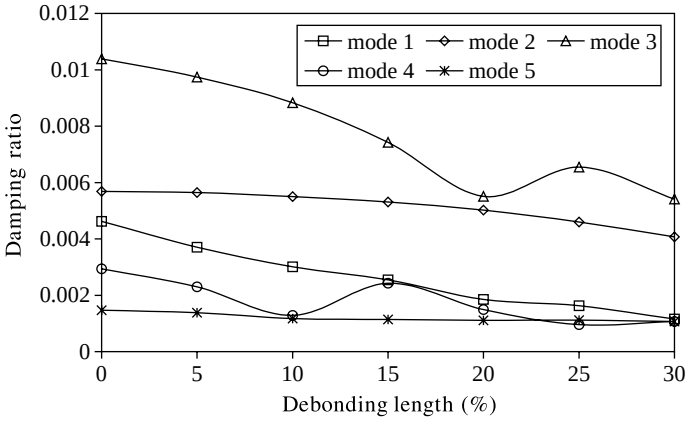

Fig. 5. Damping ratios of the open-loop system vs. debonding length.

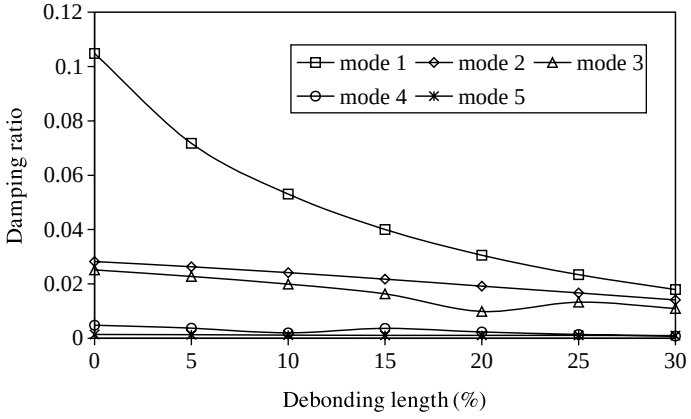

Fig. 6. Damping ratios of the closed-loop system vs. debonding length.

Finally, we examine the effects of the ACLD debonding on the active control. The hybrid (passive plus active) damping ratios of the first five modes of the closed-loop controlled beam for different debonding lengths are plotted in Fig. 6. Similar to the open-loop case, even a small debonding of the ACLD can lead to a significant reduction of the hybrid damping ratios of the controlled modes. For instance, a 10% edge debonding at the left end of the ACLD patch decreases the damping ratios for controlled four modes by 49.4%, 14.6%, 20.7% and 57.8%, respectively. Since the active control provides the control modes with active damping which can be much larger than their passive damping, the effect of the ACLD debonding on the hybrid control is more significant than the passive. As shown in Figs. 4 and 5, a 15% debonding results in a 44.8% and 6.7% reduction in passive damping for the first and second modes, but a 61.8% and 22.4% reduction in their hybrid damping in a closed-loop system. In this case, the close-loop control may be more sensitive to the ACLD debonding. To reduce the effect of ACLD debonding on active control, the controller used in the structure with perfectly treated ACLD should be carefully re-designed after debonding occurs. For instance, real-time update of the frequency in the MVO controller may improve the active control worsened by ACLD debondings.

It is interesting to note the effects of active control on the additional modes. In general, the MVO controller does not affect either the frequencies or the damping ratios of the debonding-induced additional

modes since the controller is designed to control the first four modes of the composite beam. It can be clearly seen from Table 5 that the additional mode for 25% or 30% is not affected by the MVO controller at all because its frequency is far away from the four target frequencies (i.e., 4.329, 20.744, 65.919 and 120.501). However, when the frequency of an additional mode is close to one of the target frequencies of the controller, its damping ratio will also increase since the MVO controller will treat it as a target mode. A typical example can be found in Table 5 when the debonding length is 20%. In this case, the first additional mode has a frequency of 59.95, which is close to the third target frequency of the MVO controller, its damping ratio is increased from 0.27% to 0.56% by the closed-loop control. However, the active damping effect of the controller on the third mode of the beam is remarkably weakened, as shown in Fig. 6. This is because the additional mode, which has a close frequency, shares part of the control energy.

6. Conclusion

Effects of the debonding in the ACLD patch on both passive and hybrid control of a composite beam is investigated based on a new model. In this model, both compressional and shear vibration of the VEM layer are considered to describe the debonding of in the VEM layer. In order to properly model the additional modes induced by an edge debonding with small size, the inertia and shear effects of the host beam, the piezoelectric actuator and sensor are also taken into account. A solution scheme for finding the complex eigenvalues of such a detailed model is given. The simulation example results show that an edge debonding of the ACLD patch can significantly affect the passive and hybrid control. It is also found that the additional mode induced by the debonding has unique effects on the modal damping ratios and frequencies of both open-loop and closed-loop system.

Acknowledgements

The authors are grateful to the support of the Australian Research Council through a Large Grant (Grant No. A10009074).

References

Douglas, B.E., Yang, J.C.S., 1969. Transverse compressional damping in the vibratory response of elastic–viscoelastic–elastic beam. AIAA Journal 10 (2), 163–175.

Crawley, E.F., 1994. Intelligent structures for aerospace: a technology overview and assessment. AIAA Journal 32 (8), 1689–1699.

Rao, S.S., Sunar, M., 1994. Piezoelectricity and its use in disturbance sensing and control of flexible structures: a survey. Applied Mechanics Review 47 (4), 113–123.

Chee, C., Tong, L., Steven, G.P., 1998. A review on the modelling of piezoelectric sensors and actuators incorporated in intelligent structures. Journal of Intelligent Material Systems and Structures 9 (1), 3–19.

Baz, A., 1993. Active constrained layer damping. In: Proceedings of Damping 93 San Francisco, CA.

Shen, I.Y., 1994. Hybrid damping through intelligent constrained layer treatments. Journal of Vibration and Acoustics 116, 341–349.

Shen, I.Y., 1996. Stability and controllability of Euler–Bernoulli beams with intelligent constrained layer treatments. Journal of Vibration and Acoustics 118, 70–77.

Kapadia, R.K., Kawiecki, G., 1997. Experimental evaluation of segmented active constrained layer damping treatments. Journal of Intelligent Material Systems and Structures 8 (2), 103–111.

Liao, W.H., Wang, K.W., 1997. On the analysis of viscoelastic materials for active constrained layer damping treatments. Journal of Sound and Vibration 207 (3), 319–334.

Chattopadhyay, A., Gu, H.Z., Beri, R., 2001. Modeling segmented active constrained layer damping using hybrid displacement field. AIAA Journal 39 (3), 480–486.

Shi, Y.M., Li, Z.F., Hua, H.X., Fu, Z.F., 2001. The modelling and vibration control of beams with active constrained layer damping. Journal of Sound and Vibration 245 (5), 785–800.

Lee, U., Kim, J., 2001. Spectral element modeling for the beams treated with active constrained layer damping. International Journal of Solids and Structures 38 (32–33), 5679–5702.

Seeley, C.E., Chattopadhyay, A., 1998. Experimental investigation of composite beams with piezoelectric actuation and debonding. Smart Materials and Structures 7, 502–511.

Tylikowski, A., 2001. Effects of piezo-actuator delamination on the transfer functions of vibration control systems. International Journal of Solids and Structures 38, 2189–2202.

Sun, D., Tong, L., Atluri, S.N., 2001. Effects of piezoelectric sensor/actuator debonding on vibration control of smart beams. International Journal of Solids and Structures 38 (50–51), 9033–9051.

McTavish, D.J., Hughes, P.C., 1993. Modeling of linear viscoelastic space structures. Journal of Vibration and Acoustics 115, 103–110.